



**HAL**  
open science

## **A radiomic- and dosiomic-based machine learning regression model for pretreatment planning in 177 Lu-DOTATATE therapy**

Dimitris Plachouris, Vassilios Eleftheriadis, Thomas Nanos, Nikolaos Papathanasiou, David Sarrut, Panagiotis Papadimitroulas, Georgios Savvidis, Laure Vergnaud, Julien Salvadori, Alessio Imperiale, et al.

### ► To cite this version:

Dimitris Plachouris, Vassilios Eleftheriadis, Thomas Nanos, Nikolaos Papathanasiou, David Sarrut, et al.. A radiomic- and dosiomic-based machine learning regression model for pretreatment planning in 177 Lu-DOTATATE therapy. *Medical Physics*, 2023, 50 (11), pp.7222-7235. 10.1002/mp.16746 . hal-04391726

**HAL Id: hal-04391726**

**<https://hal.science/hal-04391726>**

Submitted on 12 Jan 2024

**HAL** is a multi-disciplinary open access archive for the deposit and dissemination of scientific research documents, whether they are published or not. The documents may come from teaching and research institutions in France or abroad, or from public or private research centers.

L'archive ouverte pluridisciplinaire **HAL**, est destinée au dépôt et à la diffusion de documents scientifiques de niveau recherche, publiés ou non, émanant des établissements d'enseignement et de recherche français ou étrangers, des laboratoires publics ou privés.

# A radiomic- and dosiomic-based machine learning regression model for pretreatment planning in $^{177}\text{Lu}$ -DOTATATE therapy

Dimitris Plachouris<sup>1</sup> | Vassilios Eleftheriadis<sup>2</sup> | Thomas Nanos<sup>1</sup> | Nikolaos Papathanasiou<sup>3</sup> | David Sarrut<sup>4</sup> | Panagiotis Papadimitroulas<sup>2</sup> | Georgios Savvidis<sup>2</sup> | Laure Vergnaud<sup>4</sup> | Julien Salvadori<sup>5</sup> | Alessio Imperiale<sup>5</sup> | Dimitrios Visvikis<sup>6</sup> | John D. Hazle<sup>7</sup> | George C. Kagadis<sup>1,7</sup>

<sup>1</sup>3DMI Research Group, Department of Medical Physics, School of Medicine, University of Patras, Rion, Greece

<sup>2</sup>Bioemission Technology Solutions – BIOEMTECH, Athens, Greece

<sup>3</sup>Department of Nuclear Medicine, School of Medicine, University of Patras, Rion, Greece

<sup>4</sup>CREATIS, CNRS, Université de Lyon, Lyon, France

<sup>5</sup>Institut de cancérologie Strasbourg Europe, Strasbourg, France

<sup>6</sup>LaTIM, INSERM, UMR1101, Camille Desmoulins Av. 22, Brest, France

<sup>7</sup>Department of Imaging Physics, The University of Texas MD Anderson Cancer Center, Houston, Texas, USA

## Correspondence

George C. Kagadis, 3DMI Research Group, Department of Medical Physics, School of Medicine, University of Patras, Rion GR 26504, Greece.  
Email: [gkagadis@gmail.com](mailto:gkagadis@gmail.com) / [kagadis@upatras.gr](mailto:kagadis@upatras.gr)

## Funding information

European Union's Horizon 2020 research and innovation programme; European Regional Development Fund; Hellenic Foundation for Research and Innovation

## Abstract

**Background:** Standardized patient-specific pretreatment dosimetry planning is mandatory in the modern era of nuclear molecular radiotherapy, which may eventually lead to improvements in the final therapeutic outcome. Only a comprehensive definition of a dosage therapeutic window encompassing the range of absorbed doses, that is, helpful without being detrimental can lead to therapy individualization and improved outcomes. As a result, setting absorbed dose safety limits for organs at risk (OARs) requires knowledge of the absorbed dose–effect relationship. Data sets of consistent and reliable inter-center dosimetry findings are required to characterize this relationship.

**Purpose:** We developed and standardized a new pretreatment planning model consisting of a predictive dosimetry procedure for OARs in patients with neuroendocrine tumors (NETs) treated with  $^{177}\text{Lu}$ -DOTATATE (Lutathera). In the retrospective study described herein, we used machine learning (ML) regression algorithms to predict absorbed doses in OARs by exploiting a combination of radiomic and dosiomic features extracted from patients' imaging data.

**Methods:** Pretreatment and posttreatment data for 20 patients with NETs treated with  $^{177}\text{Lu}$ -DOTATATE were collected from two clinical centers. A total of 3412 radiomic and dosiomic features were extracted from the patients' computed tomography (CT) scans and dose maps, respectively. All dose maps were generated using Monte Carlo simulations. An ML regression model was designed based on ML algorithms for predicting the absorbed dose in every OAR (liver, left kidney, right kidney, and spleen) before and after the therapy and between each therapy session, thus predicting any possible radiotoxic effects.

**Results:** We evaluated nine ML regression algorithms. Our predictive model achieved a mean absolute dose error (MAE, in Gy) of 0.61 for the liver, 1.58 for the spleen, 1.30 for the left kidney, and 1.35 for the right kidney between pretherapy  $^{68}\text{Ga}$ -DOTATOC positron emission tomography (PET)/CT and post-therapy  $^{177}\text{Lu}$ -DOTATATE single photon emission (SPECT)/CT scans. The best predictive performance observed was based on the gradient boost for the liver, the left kidney and the right kidney, and on the extra tree regressor for the

This is an open access article under the terms of the [Creative Commons Attribution-NonCommercial](https://creativecommons.org/licenses/by-nc/4.0/) License, which permits use, distribution and reproduction in any medium, provided the original work is properly cited and is not used for commercial purposes.

© 2023 The Authors. Medical Physics published by Wiley Periodicals LLC on behalf of American Association of Physicists in Medicine.

spleen. Evaluation of the model's performance according to its ability to predict the absorbed dose in each OAR in every possible combination of pretherapy  $^{68}\text{Ga}$ -DOTATOC PET/CT and any posttherapy  $^{177}\text{Lu}$ -DOTATATE treatment cycle SPECT/CT scans as well as any  $^{177}\text{Lu}$ -DOTATATE SPECT/CT treatment cycle and the consequent  $^{177}\text{Lu}$ -DOTATATE SPECT/CT treatment cycle revealed mean absorbed dose differences ranges from  $-0.55$  to  $0.68$  Gy. Incorporating radiodosimics features from the  $^{68}\text{Ga}$ -DOTATOC PET/CT and first  $^{177}\text{Lu}$ -DOTATATE SPECT/CT treatment cycle scans further improved the precision and minimized the standard deviation of the predictions in nine out of 12 instances. An average improvement of 57.34% was observed (range: 17.53%–96.12%). However, it's important to note that in three instances (i.e., Ga,C.1  $\rightarrow$  C3 in spleen and left kidney, and Ga,C.1  $\rightarrow$  C2 in right kidney) we did not observe an improvement (absolute differences of 0.17, 0.08, and 0.05 Gy, respectively). Wavelet-based features proved to have high correlated predictive value, whereas non-linear-based ML regression algorithms proved to be more capable than the linear-based of producing precise prediction in our case.

**Conclusions:** The combination of radiomics and dosimics has potential utility for personalized molecular radiotherapy (PMR) response evaluation and OAR dose prediction. These radiodosimic features can potentially provide information on any possible disease recurrence and may be highly useful in clinical decision-making, especially regarding dose escalation issues.

#### KEYWORDS

$^{177}\text{Lu}$ -DOTATATE, dose prediction model, dosimetry, dosimics, machine learning, radiomics, radiotoxicity, regression model, treatment planning

## 1 | INTRODUCTION

Molecular radiotherapy (MRT) uses radioactive sources to treat cancer<sup>1–3</sup> by delivering a radioactive radioisotope directly to the tumorous area.<sup>4</sup> In MRT prior to treatment, a planning agent is administered either for dosimetry or patient selection purposes.<sup>5,6</sup> MRT protocols focus on ensuring a treatment is safe, rather than on determining the absorbed dose for a particular patient population. That may lead to possible undertreatment or overtreatment.<sup>7–10</sup> Despite being used for decades, no clear formula exists yet to link the radioactivity of the injected radiopharmaceutical with the absorbed dose in the recipient's tissues.

Neuroendocrine tumors (NETs) mostly arise from endocrine cells of the embryological midgut.<sup>11</sup> NETs are at an advanced stage (disseminated metastasis) in up to 25% of patients<sup>12</sup> at presentation and are often detected during surgery for bowel obstruction, perforation, or bleeding.<sup>13</sup> Establishing a well-validated pretreatment prognostic protocol for NETs and guiding NET patients toward the most appropriate course of therapy are both challenging.

For treating NETs, somatostatin receptor (SSTR) agonists labeled with  $^{68}\text{Ga}$  ( $^{68}\text{Ga}$ -DOTA-SSA) are used in positron emission tomography (PET) to diagnose and select suitable candidates for treatment. SSTRs targeted with  $^{177}\text{Lu}$ -DOTATATE are then used for peptide receptor radionuclide therapy (PRRT)

in SSTR-expressing tumors.<sup>2</sup> The  $^{177}\text{Lu}$ -DOTATATE PRRT application has shown positive effects on small intestinal NETs in the NETTER-1 trial, with better objective responses and increased progression-free survival durations than octreotide treatment.<sup>14–16</sup> To increase the absorbed dose while preserving organs at risk (OARs) two main options of injecting  $^{177}\text{Lu}$ -DOTATATE have been proposed:<sup>15,17</sup> (1) a fixed four-cycle regimen with 7.4 GBq/cycle, reassuring safety based on the extrapolated dose limits from external beam radiation therapy (EBRT), and (2) a varying number of cycles with or without variable activity per cycle until OARs absorb preset doses,<sup>9</sup> with the first being more prevalent.

New findings supported the critical significance of nuclear imaging in not only NET patient selection for PRRT but also assessment of treatment response. Authors discovered a dose–response association between the absorbed dose in PRRT and tumor shrinkage in both small intestinal and pancreatic NET patients, with the association being more prominent in the latter.<sup>18</sup>

Radiomics<sup>19,20</sup> is a new potential topic of study that has emerged as a result of the introduction of new technologies in imaging and the demands of precision medicine.<sup>21</sup> Researchers have widely exploited radiomic characteristics in this respect for cancer prognosis and subtyping and lesion/tissue characterization.<sup>22</sup> In addition to the radiomic approach to identify quantitative biomarkers, other groups investigated a dosimic approach, which is designed to extract spatial aspects

of the dose distribution in various imaging approaches. While dosiomics has been extensively studied in EBRT,<sup>23,24</sup> its application in nuclear medicine (NM) has been relatively limited. However, there is a growing interest in combining radiomics and dosiomics approaches lately to achieve a more comprehensive and accurate assessment of treatment response and prognosis in cancer patients.<sup>25–28</sup>

As previously described, NETs typically respond to PRRT with disease stabilization, but the optimal sequence for PRRT is not yet determined due to challenges in targeting multiple tumors in the midgut area. Dosimetric evaluation is mainly focused on protecting vital organs, and developing tailored therapy regimens to minimize radiotoxic damage to these organs. Personalizing NET treatment is crucial, and recent advances in artificial intelligence (AI) techniques offer promising applications. In nuclear medicine, a one-size-fits-all treatment planning technique is no longer appropriate.<sup>29–31</sup> Accurate dose prediction is important for optimizing clinical plans, and AI has proven to be an effective tool for predicting therapy response and guiding tailored therapy planning in the future.<sup>32–34</sup>

ML and deep learning (DL) models have started being used to address the challenge of personalized pretreatment planning in nuclear medicine, with promising results.<sup>21,35,36</sup> Furthermore, researchers have investigated the predictive usefulness of SSTR-expressing tumor agonists labeled with several radioisotopes, including <sup>177</sup>Lu-DOTATATE.

In the study conducted by Chicheportiche et al.,<sup>37</sup> they used linear regression analysis focusing on the relationship between the absorbed dose of the first cycle and those of subsequent cycles on the kidneys. They did not evaluate posttreatment dose prediction or any correlations among OARs.<sup>37</sup> Also, they did not assess the ability of the pretreatment baseline PET/CT scans to predict the posttreatment absorbed dose, even though it has been shown to be useful for more than only selection purposes. Several studies suggest that the quantitative measurements obtained from pretreatment PET/CT scans using <sup>68</sup>Ga-DOTA peptides and standard uptake value (SUV) could be indicative of the absorbed dose to the tumor<sup>38,39</sup> or the OARs during PRRT.<sup>40–45</sup> Kim et al. presented results of a study of 13 patients investigating the predictive value of <sup>68</sup>Ga-DOTATOC PET/CT scan in a linear regression analysis.<sup>44</sup> They presented a general mathematical formula which was based on the mean SUV in <sup>68</sup>Ga-DOTATOC PET/CT scans for predicting the absorbed dose on critical organs (tumor, kidneys, liver, and bone marrow) after treatment with <sup>177</sup>Lu-DOTATATE without assessing any potential relationships between any possible treatment sessions. On the other hand, Ezziddin et al.<sup>43</sup> found that the pretreatment SUV of <sup>68</sup>Ga-DOTATOC PET scans could predict the absorbed dose in tumors after cycle 1 in 21 patients treated for NETs with <sup>177</sup>Lu-Octreotate.

None of these investigators studied any correlations among OARs. However, Thuillier et al.<sup>42</sup> conducted a study involving 10 NETs patients, in which they found a correlation between several SUV-based parameters on <sup>68</sup>Ga-DOTATOC PET and <sup>177</sup>Lu-DOTATATE SPECT scans acquired 24 h after cycle 1. The correlation pertained to SUV ratios among the tumor, liver, and spleen. Similarly, Wong et al.<sup>45</sup> observed a correlation between pretherapy <sup>68</sup>Ga-DOTATATE PET and post-therapy <sup>177</sup>Lu-DOTATATE SPECT SUV tumor-to-normal organ ratios (liver, spleen, and kidneys) in 24 patients at 4 and 24 h after cycle 1. These studies provide evidence of the potential usefulness of pretherapeutic scans for predicting posttreatment doses or for establishing correlations between post- and pretreatment scans in patients undergoing treatment for NETs.

In the present retrospective study, we assessed a new machine learning (ML)-based pretreatment planning model for predicting the dosimetry in OARs in NET patients undergoing therapy with <sup>177</sup>Lu-DOTATATE (Lutathera®). We standardized our model which can be used for the absorbed dose prediction in each OAR over four <sup>177</sup>Lu-DOTATATE treatment cycles and consequently prevent radiotoxicity and optimize the standard clinical practice. We used a combination of radiomic and dosiomic features extracted from patients' imaging data. Identifying these radiodosiomic features (dose signatures or dose expression patterns) may provide information on treatment prediction of NETs and may be highly useful in clinical decision-making, especially regarding dose escalation issues.

## 2 | MATERIALS AND METHODS

### 2.1 | Clinical patient cohort

To extend our training data set and generalize it as much possible, our ML model was trained with a data set for a total of 20 NET patients at two institutions. The first data set was for 12 patients who received treatment from November 2018 to March 2021 at Centre Léon-Bérard Center (Lyon, France), whereas the second was for eight patients who received treatment from July 2020 to September 2021 at the Institut de cancérologie Strasbourg Europe (Strasbourg, France). All 20 patients underwent PRRT with <sup>177</sup>Lu-DOTATATE. The first group consisted of eight female and four male patients. Eleven of these patients had hepatic metastases, six had peritoneal metastatic disease, five had lymph node metastases, three had metastatic bone lesions, and two had pancreatic metastatic disease. The mean ( $\pm$  SD) radioactivity of <sup>177</sup>Lu-DOTATATE injected in these patients was 6832 ( $\pm$  158) MBq. The second group consisted of three female and five male patients. All eight patients had hepatic metastases, seven had peritoneal metastatic disease, four had metastatic bone

lesions, two had lymph node metastases, and two had pancreatic metastatic disease. The mean ( $\pm$ SD) radioactivity of injected  $^{177}\text{Lu}$ -DOTATATE in this group was 7222 ( $\pm$ 113) MBq.

Physicians at both institutions followed the same therapeutic protocol. Almost all patients underwent four treatment cycles with about 8-week gaps between cycles, except two patients. Specifically, patient 1 had a time frame of 28 weeks between cycles 3 and 4, while patient 9 had 24 weeks between cycles 2 and 3 and an injected activity equal to 3428 MBq for cycle 3. We did not have access to additional demographic data due to institutional constrictions. Overall, the complete data set for these 20 patients consisted of a total of 186 data sets (from computed tomography [CT] and nuclear scans); data sets for 20 pretherapy  $^{68}\text{Ga}$ -DOTATOC PET/CT and 73 posttherapy  $^{177}\text{Lu}$ -DOTATATE single photon emission CT (SPECT)/CT scans were collected. Specifically, concerning the posttherapy  $^{177}\text{Lu}$ -DOTATATE SPECT/CT scans, the data set consisted of 20 cycle 1 scans, 18 cycle 2 scans, 17 cycle 3 scans, and 18 cycle 4 scans. A few data were missing in cases in which the physicians decided the patients should not complete all of the treatment cycles (based on the patients' hematological or histological examinations or overall clinical condition), or SPECT/CT could not be performed owing to technical reasons attributed to the COVID-19 pandemic. Patients 3 and 4 stopped the treatment after the second cycle. For patient 5, posttreatment SPECT/CT scans of cycles 2 and 3 and for patient 11 SPECT/CT scans of cycle 2 were not available. The image segmentation and reconstruction protocols are analytically detailed in Vergnaud et al.<sup>46</sup> Briefly, all acquisitions were performed with the GE Discovery NM CT 670 (first dataset) or GE Discovery NM CT 870 DR (second dataset) with MEGP collimators, in 15 (first dataset) or 20 (second dataset) minutes. Reconstructions were performed with OSEM, eight iterations and eight subsets, with DEW scatter correction, attenuation correction, and resolution recovery (depth-varying PSF). Calibration for detected counts in MBq/mL was performed according to the MIRD 23 protocol.<sup>47</sup> For the purpose of the present study, we used the post-injection SPECT/CT scans that were planned at 24 h post every treatment cycle. All OARs (liver, kidneys, and spleen) were manually segmented by two experienced oncologists.

## 2.2 | ML regression model

To train a ML model for predicting the absorbed doses in the patients' OARs over time (treatment cycle), our data set had to be restructured into pairs of starting and ending treatment session time points, classifying our ML model as a regression-type one. The input domain fed

to the ML model consisted of the continuous dosimetric features extracted from each of the pretherapy dose biodistribution maps. These features were collected over the whole therapy procedure as well as from the starting time point to the ending time point for each treatment cycle and combined with the patients' anatomical characteristics (radiomics). The absorbed OAR dose at the ending time point for each posttreatment treatment cycle was set as the output of the model. Determining the best combination of biomarkers acquired from the initial  $^{68}\text{Ga}$ -DOTATOC PET/CT images for predicting absorbed dose to OARs in any of the PRRT cycles was one of the study's primary goals. Various combinations of features were taken into consideration by using image-derived biomarkers and other pertinent factors (patient weight and height and injected radioactivity of radiopharmaceuticals used). Multivariate analysis was performed to discard any biomarkers that did not provide complementary information and, as a result, identify the combination of features that provided the maximum stratification correlation for the pretreatment and posttreatment imaging sessions.

Because the study treatment lasted more than 30 weeks overall (the time frame for all four cycles and breaks between them), the ability of our regression model to predict the absorbed dose in each OAR was evaluated over each treatment cycle. The proposed model generates four continuous dose values representing the predicted absorbed dose in each of the four treatment cycles of  $^{177}\text{Lu}$ -DOTATATE when the input is based on the features extracted from the  $^{68}\text{Ga}$  DOTATOC pretreatment scans. If the model is fed with additional dose information as the therapy progresses, it can lead to updated dose values for the cycles that will follow. For example, if the input features include information from cycle 1, the output will include predictions for cycles 2, 3, and 4. The same applies if features from multiple cycles are included in the input, where the output will only include predictions for the remaining cycles (presented at Figures 2 and 3, in the Results section). Finally, an additional goal was to identify which radiodosimetrics are optimal and the appropriate feature selection method for the creation of an overall predictive model of therapy response over the course of the four cycles of PRRT.

Nine supervised linear and non-linear-based ML regression algorithms were evaluated: linear regression, ridge regression, extra tree regression, AdaBoost regression, gradient boost regression, random forest regression, decision tree regression, support vector regression (SVR),<sup>48</sup> and XGBoost regression.<sup>49</sup> These algorithms are considered state-of-the-art for classification and regression problems. The ML regression model was built using the Python programming language (v.3.10.2).<sup>50</sup>

## 2.3 | Training parameters

### 2.3.1 | Feature extraction

In total, 3412 radiodosiomic features were used to characterize all OARs in both the CT images and the dose maps for each image data set (pretherapy  $^{68}\text{Ga}$ -DOTATOC and posttherapy  $^{177}\text{Lu}$ -DOTATATE treatment cycles' scans). These features cover the whole spectrum of the PyRadiomics library<sup>51</sup> for all conceivable multimodal images used in  $^{177}\text{Lu}$ -DOTATATE treatment planning in clinical practice (PET, SPECT, and CT scans). Specifically, radiomics' and dosiomics' features were extracted from every possible feature class (First Order, GLCM, GLDM, GLRLM, GLSZM, NGTDM, Shape, and Shape2D and their corresponding wavelet-based features). In addition to the radiomics extracted from the patients' anatomical characteristics, our model was fed with the patients' body mass index values (weight and height). Also, extraction settings that were consistent with the most up-to-date benchmark values according to the Image Biomarker Standardization Initiative guidelines (IBSI)<sup>52</sup> were chosen. All features were extracted with a fixed bin and voxel size. The voxel size was set to  $1 \times 1 \times 1 \text{ mm}^3$  and discretization was set to 64 bins. Additionally, before the feature selection process (see Section 2.3.2), all extracted features were normalized as shown in Equation (1) to produce a scaled training data set with zero mean variability and unit variance.

$$z = \frac{\chi - \mu}{\sigma} \quad (1)$$

$$z = \frac{x - \frac{1}{N} \sum_{i=1}^N (x_i)}{\sqrt{\frac{\sum_{i=1}^N (x_i - \mu)^2}{N}}}$$

In this equation,  $\chi$  is the radiodosiomic feature,  $\mu$  is the mean value of all radiodosiomic features,  $\sigma$  is the SD for this mean value, and  $N$  is the total number of radiodosiomic features.

### 2.3.2 | Feature selection

Owing to the high-dimensional data set produced via PyRadiomics library<sup>51</sup> feature extraction, feature selection is a critical stage in the workflow of a radiomics-based study.<sup>53,54</sup> A mixture of feature selection strategies was employed in the present study. To meaningfully reduce the dimensionality of our training data set and select robust features, initially, two filter-based feature selection techniques were used: an unsupervised univariate analysis of the association among the radiodosiomic features (Pearson's correlation coefficient)<sup>55</sup> and a supervised multivariate analysis of the association between the radiodosiomic features and the

target feature (in our case the absorbed dose to a specific OAR) (mutual information criterion).<sup>56</sup> Additionally, two wrapper techniques (the feature sequential backward elimination [SBS] and the forward recursive feature elimination [RFE])<sup>48</sup> were applied to find the best feature combination for each of the ML regression algorithms that we tested for every OAR. Figure 1 shows a schematic of the feature selection process that we used. Also, two ML regression algorithms that leverage embedded feature selection approaches (the XGBoost and ridge regression algorithms) were included in our experiments.<sup>48,49</sup> Specifically, the mutual information criterion, which is shown in Equation (2), was used to quantify the mutual reliance between the target value and the remainder of the derived radiodosiomic features.

$$I(X; Y) = D_{KL}(P_{(X,Y)} \| P_{Y \otimes P_X}) \quad (2)$$

In this equation,  $(X, Y)$  represents a pair of random variables with  $P_{(X,Y)}$  as their joint distribution and  $P_X$  and  $P_Y$  as their marginal distributions.  $D_{KL}$  is the Kullback–Leibler divergence.<sup>57</sup> All features having a mutual information score lower than 0.3 were removed from the data set as they were considered irrelevant to the predictive assignment.

To quantify the degree and direction of the linear relationships among all pairs of the remaining features, the unsupervised Pearson's correlation coefficient was used<sup>55</sup> as shown in Equation (3)

$$\rho_{X,Y} = \frac{\text{cov}(X, Y)}{\sigma_X \sigma_Y}$$

$$\rho_{X,Y} = \frac{\mathbb{E}[(X - \mu_X)(Y - \mu_Y)]}{\sigma_X \sigma_Y} \quad (3)$$

where  $(X, Y)$  represents a pair of random variables with  $\text{cov}_{(X,Y)}$  as their covariance, which can be expressed as their expectation ( $\mathbb{E}$ ). Also,  $\mu$  and  $\sigma$  represent the mean value and SD, respectively.

Highly correlated features with an absolute Pearson's correlation coefficient value greater or equal to 0.8 were compared with one another. Features with an absolute Pearson's correlation coefficient value lower than 0.8 were considered redundant and excluded from the data set.

The wrapper technique described above was employed at the final phase of the feature selection process to find the feature subset that leads to the best predicted performance for each of the ML algorithms. Furthermore, because wrapper approaches are algorithm-specific, the feature selection procedures for each combination of the remaining radiodosiomic features and ML algorithms were performed independently.

The embedded feature selection approaches were the last steps in the feature selection process. They were implemented in algorithms with their own built-in feature selection methods. If an algorithm failed to produce valid

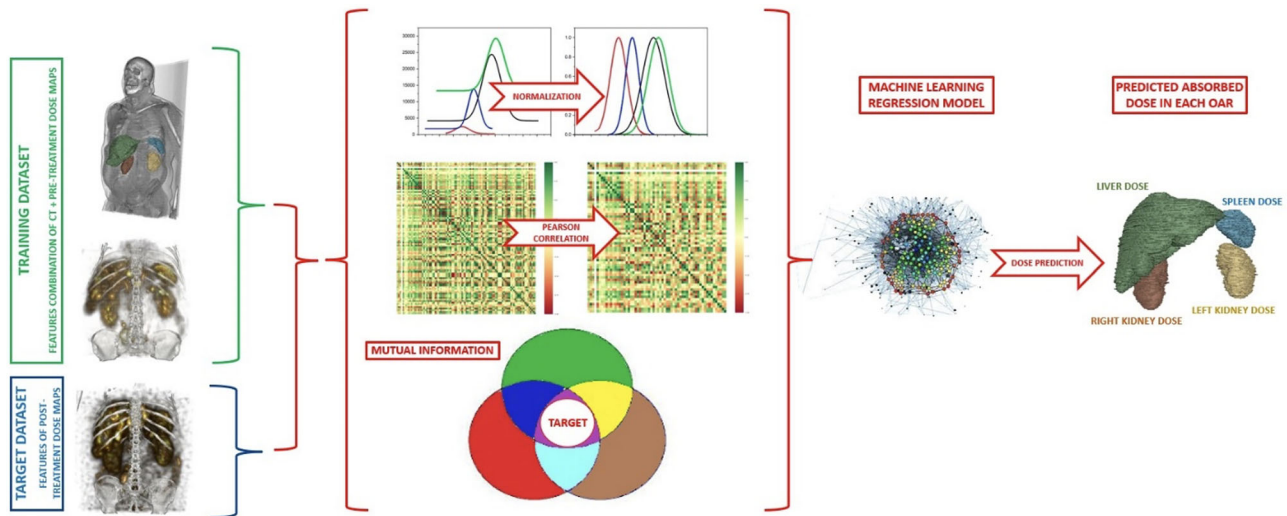


**FIGURE 1** Schematic of the ML model's workflow.

results in selecting more than 10 features, it indicated overfitting (following the 10:1 rule of thumb). Consequently, the algorithm's results were not evaluated.

## 2.4 | Validation methods and metrics

To train and validate the model, leave-one-out cross-validation<sup>58</sup> was used. This approach was chosen primarily to compensate for the small sample size. Leave-one-out cross-validation enabled us to train the model with more data than that with any other training and validation method. For performance comparison and optimization reasons, mean absolute error<sup>59</sup> was employed as the major model performance metric to assess the prediction performance of each of our ML regression algorithms.

Dose maps generated through direct full Monte Carlo (MC) simulations were used as the references. The predicted dose values for each OAR were evaluated and validated in comparison with the dose values that were extracted from the ground truth dose maps. The ground truth dose maps were based on SPECT/CT scans taken 24 h after each treatment cycle and generated using the GATE v.9.0 MC simulation toolkit.<sup>60</sup> To simulate the radioisotope voxelized source distribution and the patients' anatomical characteristics, patient PET/SPECT and CT data, respectively, were imported into GATE, and the generated dose maps were registered to the patients' CT scans. The GATE database<sup>60,61</sup> was used to convert CT Hounsfield units into densities. The physical processes were simulated using the standard electromagnetic emstandard\_opt4 physics package of the Geant4 10.6 software application, and every <sup>177</sup>Lu particle's interaction at each voxel with a specific material composition was simulated using the

<sup>177</sup>Lu continuous spectrum ranging from 0 to 0.498 MeV, with a mean energy of 0.149 MeV, half-life of 6.647 days and a tissue penetration range up to 2.2 mm.<sup>2</sup> The voxel size of the 3D generated dose maps was set to  $1 \times 1 \times 1 \text{ mm}^3$  in order to have a high resolution in dose deposition, considering the Beta emission contribution. In every simulation, to reach a sufficiently low level of statistical uncertainty,  $5 \times 10^9$  primary events were simulated. The achieved mean statistical uncertainty was almost  $\sim 2\%$  for each OAR (liver, left and right kidneys, and spleen) in every patient. All simulations were executed in the "YOTTA Advanced Computing" high-performance computing (HPC) center.<sup>62</sup>

Differences in the absorbed dose values for each OAR were analyzed in terms of relative and absolute differences. The mean absorbed dose differences in every OAR were reported by calculating the mean value of the absorbed dose and the absolute absorbed dose differences in every OAR.

To assess the prediction performance of our ML regression model across all treatment cycles, we calculated five different performance metrics. The mean absolute error (MAE), the root mean square error (RMSE), the R-squared ( $R^2$ ), the mean percentage error (MPE), and the mean relative error (MRE).<sup>59,63</sup> Because MAE, RMSE, MPE, and MRE are scale dependent, they can be used to assess the performance of various predictive regression models for a given dataset, whereas  $R^2$  indicates the fraction of the variation of the target value explained by the input characteristics in a regression model. From the selected metrics, MAE was employed as the major model performance metric in this study for performance comparison and optimization reasons. MAE and RMSE metrics are calculated in Gy. Differences in the absorbed dose values for each OAR were analyzed in terms of absolute dose differences.

**TABLE 1** Regression evaluation metrics (MAE, RMSE and MRE in Gy, and MPE in %) of the best performing regression algorithm for each OAR.

OARs	Regression algorithm	Regression evaluation metrics				
		MAE	RMSE	R <sup>2</sup>	MPE	MRE
Liver	Gradient Boost	0.61	0.89	0.63	-17.95	0.34
Spleen	Extra Tree Regressor	1.58	2.08	0.54	-13.56	0.33
Left kidney	Gradient Boost	1.30	1.70	0.60	-9.64	0.30
Right kidney	Gradient Boost	1.35	1.70	0.65	-16.11	0.37

### 3 | RESULTS

We evaluated the ability of nine ML-based regression algorithms to predict the absorbed dose in every OAR (liver, spleen, and left and right kidneys) using pretherapy <sup>68</sup>Ga-DOTATOC PET/CT and posttherapy <sup>177</sup>Lu-DOTATATE SPECT/CT scans following every treatment cycle. We extracted the real dose values for each OAR from MC simulations, and as indicated, we considered these dose values the ground truth for every comparison with our generated model's predicted dose values. We also evaluated our model's performance in predicting the total cumulative absorbed dose in each OAR for every patient over the course of all four treatment cycles.

#### 3.1 | Evaluation of the performance of the best ML-based model

Overall, the best predictive algorithms with the pretherapy <sup>68</sup>Ga-DOTATOC PET/CT and posttherapy <sup>177</sup>Lu-DOTATATE SPECT/CT scans achieved mean dose absolute error of 0.61, 1.58, 1.30, and 1.35 for the liver, spleen, left kidney, and right kidney, respectively. Analytical results for the best performing regression algorithm for each OAR are presented in Table 1.

As shown in Table 1, none of the regression algorithms outperformed the others in predictive performance for all OARs.

#### 3.2 | Evaluation of the performance of the model in predicting the absorbed dose among all treatment cycles

We evaluated the best performing regression algorithm for each OAR according to its ability to predict the absorbed dose in every possible combination of pretherapy <sup>68</sup>Ga-DOTATOC PET/CT and any posttherapy <sup>177</sup>Lu-DOTATATE treatment cycle SPECT/CT scans as well as any <sup>177</sup>Lu-DOTATATE SPECT/CT treatment cycle and the consequent <sup>177</sup>Lu-DOTATATE SPECT/CT treatment cycle scans. In the following tables and figures, "Ga" stands for pretherapy <sup>68</sup>Ga-DOTATOC scans, "C" stands for posttherapy <sup>177</sup>Lu-DOTATATE scans, and the

arrow symbol shows the direction of prediction, that is, the left part is the input that predicts the output, right part. Also, "C" is followed by the corresponding treatment cycle number. In Figure 2, the mean differences in the predicted absorbed dose are illustrated. A more detailed analysis is depicted in Figure 3.

Incorporating information from previous treatment cycles as inputs led to improved and consistently more stable outcomes in most ML regression algorithms. This effect was particularly pronounced when combining data from the first treatment cycle with information from the pretreatment cycle. For example, for the left kidney, the mean ( $\pm$ SD) dose difference from Ga→C.4 was  $0.21 \pm 2.30$  Gy, and that from (Ga, C.1)→C.4 was  $-0.01 \pm 1.47$  Gy. The analytical results of all possible combinations are presented in Table 2.

As it can be seen in Table 2, incorporating radiodosimics features from the <sup>68</sup>Ga-DOTATOC PET/CT and first <sup>177</sup>Lu-DOTATATE SPECT/CT treatment cycle scans further improved the precision and minimized the standard deviation of the predictions in nine out of 12 instances. An average improvement of 57.34% was observed (range: 17.53%–96.12%). However, it is important to note that in three instances (i.e., Ga,C.1 → C3 in spleen and left kidney, and Ga,C.1 → C2 in right kidney) we did not observe an improvement (absolute differences of 0.17, 0.08, and 0.05 Gy, respectively).

#### 3.3 | Final selected features

One of the main objectives of this study was to identify radiodosimic signatures that can facilitate the use of anatomical and dose features for predicting the absorbed dose escalation over the course of four <sup>177</sup>Lu-DOTATATE treatment cycles. In Table 3, the final selected radiodosimic features from among the 3412 initial extracted features for the four OARs are listed.

As described above, we trained and evaluated nine ML algorithms for every OAR. Therefore, the final selected features differed for each OAR. The Recursive Feature Elimination (RFE) method consistently exhibited superior interpretability in comparison to Sequential Backward Selection (SBS) across all the final best algorithms. The utilization of RFE allowed

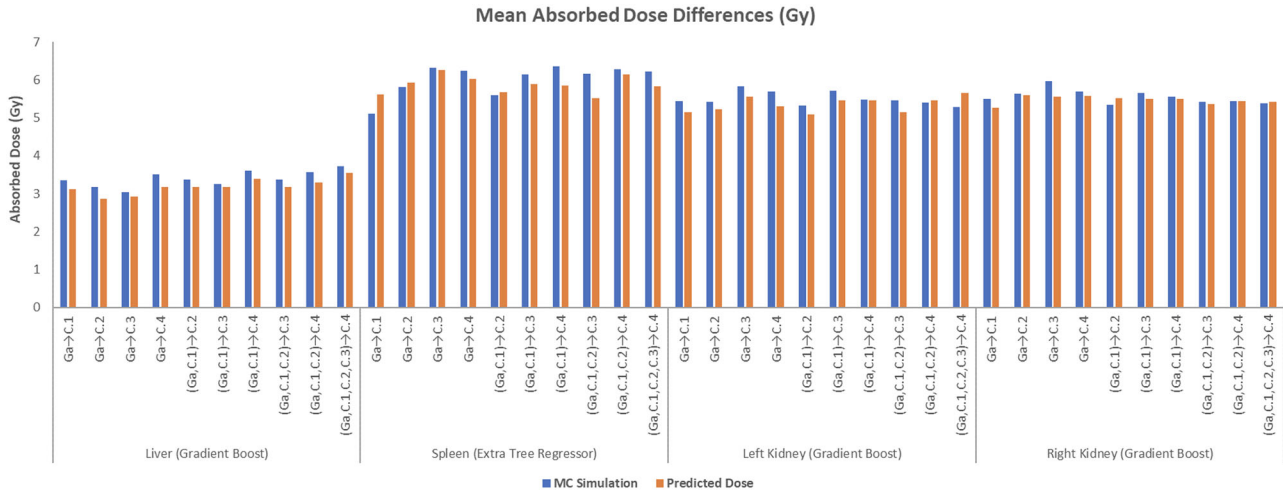


**FIGURE 2** Comparison of MC simulations and mean predicted absorbed dose (in Gy) for every OAR in all patients. Ga, pretherapy  $^{68}\text{Ga}$ -DOTATOC scans; C, posttherapy  $^{177}\text{Lu}$ -DOTATATE scans.

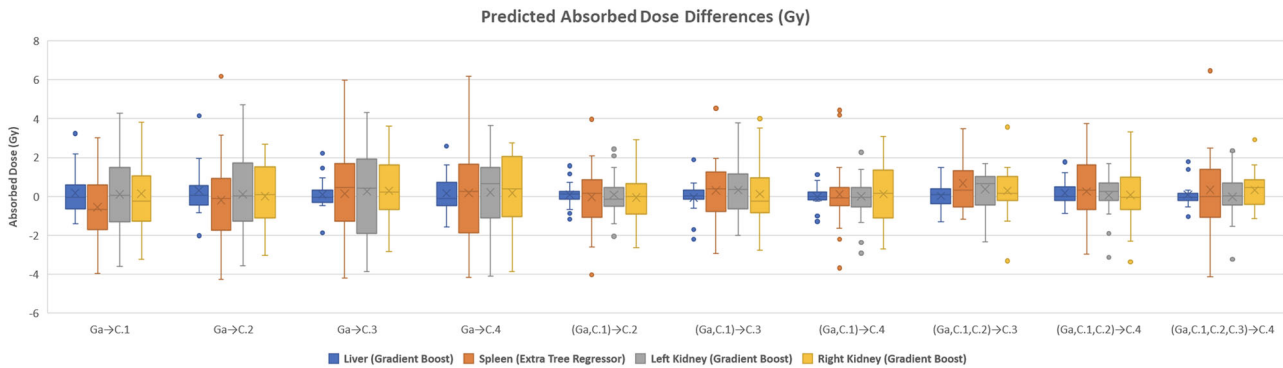


**FIGURE 3** Box-and-whisker plots of the predicted absorbed dose differences in every OAR for every possible combination of scans for the pretreatment and posttreatment cycles. Ga, pretherapy  $^{68}\text{Ga}$ -DOTATOC scans; C, posttherapy  $^{177}\text{Lu}$ -DOTATATE scans.

**TABLE 2** Differences between the predicted absorbed dose values and ground truth (MC simulations) for every pretreatment and posttreatment imaging session in all OARs.

Treatment cycles <sup>a,b</sup>	Absorbed dose difference (Gy)							
	Liver		Spleen		Left kidney		Right kidney	
	Mean [95% CI]	SD	Mean [95% CI]	SD	Mean [95% CI]	SD	Mean [95% CI]	SD
Ga→C.1	0.17 [−0.37, 0.98]	1.10	−0.55 [−1.39, 0.34]	1.95	0.11 [−0.74, 0.95]	1.90	0.14 [−0.64, 1.01]	1.91
Ga→C.2	0.30 [−0.37, 0.98]	1.35	−0.19 [−1.45, 1.06]	2.52	0.11 [−1.03, 1.24]	2.29	−0.01 [−0.72, 1.01]	1.70
Ga→C.3	0.09 [−0.36, 0.54]	0.88	0.14 [−1.19, 1.41]	2.54	0.25 [−1.19, 1.27]	2.45	0.29 [−0.77, 1.13]	1.78
Ga→C.4	0.16 [−0.30, 0.62]	0.98	0.17 [−1.10, 1.43]	2.71	0.21 [−0.76, 1.15]	2.03	0.17 [−0.75, 1.24]	1.97
(Ga,C.1)→C.2	0.09 [−0.24, 0.42]	0.66	−0.03 [−0.88, 0.99]	1.81	0.09 [−0.54, 0.72]	1.27	−0.06 [−0.96, 0.63]	1.60
(Ga,C.1)→C.3	−0.05 [−0.51, 0.40]	0.89	0.31 [−0.57, 1.20]	1.72	0.33 [−0.48, 1.13]	1.57	0.12 [−0.90, 1.04]	1.86
(Ga,C.1)→C.4	−0.02 [−0.31, 0.27]	0.62	0.11 [−0.81, 1.02]	1.95	0.01 [−0.68, 0.70]	1.47	0.12 [−0.80, 0.63]	1.66
(Ga,C.1,C.2)→C.3	0.03 [−0.37, 0.43]	0.75	0.68 [−0.16, 1.52]	1.57	0.37 [−0.18, 0.92]	1.03	0.29 [−0.34, 1.02]	1.46
(Ga,C.1,C.2)→C.4	0.17 [−0.22, 0.57]	0.74	0.26 [−0.72, 1.24]	1.84	0.06 [−0.60, 0.72]	1.23	0.07 [−0.70, 1.02]	1.65
(Ga,C.1,C.2,C.3)→C.4	0.09 [−0.25, 0.43]	0.66	0.34 [−0.84, 1.52]	2.29	−0.02 [−0.83, 0.79]	1.58	0.32 [−0.58, 1.07]	1.54

<sup>a</sup>Ga, pretherapy  $^{68}\text{Ga}$ -DOTATOC scans; C.1-4, posttherapy  $^{177}\text{Lu}$ -DOTATATE scans for cycles 1-4.

<sup>b</sup>The arrow symbol shows the direction of prediction, that is, the left part is the input that predicts the output, right part.

**TABLE 3** Radiodosiomic features producing the best results in the model's prediction accuracy (best performing algorithm in parentheses).

<b>Target organ: liver (gradient boost)</b>	
<b>Features' origin</b>	<b>Features (8)</b>
Other	Days_Between_Treatment
Liver	wavelet-HLL_firstorder_Dose_Map_Liver_Mean wavelet-LLH_gldm_Dose_Map_Liver_DependenceNonUniformityNormalized wavelet-LLL_firstorder_Dose_Map_Liver_Entropy
Spleen	original_glszm_Dose_Map_Spleen_SizeZoneNonUniformity wavelet-HHH_glszm_Dose_Map_Spleen_ZoneVariance wavelet-LLL_glszm_Dose_Map_Spleen_ZoneEntropy
Left kidney	wavelet-HLH_glszm_Dose_Map_Left_Kidney_ZoneVariance
<b>Target organ: spleen (extra tree regressor)</b>	
<b>Features (7)</b>	
Other	Days_Between_Treatment Height
Liver	original_shape_CT_Liver_MeshVolume original_shape_CT_Liver_Flatness wavelet-HHH_gldm_Dose_Map_Liver_LargeDependenceLowGrayLevelEmphasis
Spleen	wavelet-HLH_firstorder_Dose_Map_Spleen_Variance
Right kidney	wavelet-LLL_firstorder_Dose_Map_Right_Kidney_10Percentile
<b>Target organ: left kidney (gradient boost)</b>	
<b>Features (10)</b>	
Other	Days_Between_Treatment Weight Height
Liver	wavelet-HLH_gldm_Dose_Map_Liver_SmallDependenceLowGrayLevelEmphasis wavelet-HLH_glszm_Dose_Map_Liver_SmallAreaEmphasis
Spleen	wavelet-LHL_firstorder_Dose_Map_Spleen_Uniformity
Left kidney	wavelet-HLL_firstorder_Dose_Map_Left_Kidney_Mean
Right kidney	original_shape_CT_Right_Kidney_SurfaceVolumeRatio original_shape_CT_Right_Kidney_MinorAxisLength wavelet-LLH_gldm_Dose_Map_Right_Kidney_RunLengthNonUniformity
<b>Target organ: right kidney (gradient boost)</b>	
<b>Features (10)</b>	
Other	Days_Between_Treatment Height
Liver	original_gldm_Dose_Map_Liver_GrayLevelNonUniformity wavelet-LLL_gldm_Dose_Map_Liver_Idn wavelet-LLL_gldm_Dose_Map_Liver_LongRunHighGrayLevelEmphasis
Left kidney	wavelet-HLL_firstorder_Dose_Map_Left_Kidney_Mean wavelet-LLH_gldm_Dose_Map_Left_Kidney_LongRunLowGrayLevelEmphasis
Right kidney	original_shape_CT_Right_Kidney_SurfaceVolumeRatio wavelet-LLH_glszm_Dose_Map_Right_Kidney_ZonePercentage wavelet-HHH_glszm_Dose_Map_Right_Kidney_SizeZoneNonUniformityNormalized

Note: The first column lists the origin from which the features were extracted, whereas the second column lists the selected features.

us to identify and retain the most informative features while discarding less relevant ones, resulting in a more comprehensible and meaningful representation of the OARs' impact on the chosen algorithms. This facilitated more insightful analysis and decision-making in the context of organ-at-risk considerations.

## 4 | DISCUSSION

PRRT using radiolabeled SSTR agonists is a well-tolerated treatment for NETs, but reliable data on long-term adverse consequences are limited.<sup>64–67</sup>

The aim of the present research was to study the feasibility of utilizing dosiomics features, as those have been successfully exploited in EBRT and uncover radiodosiomic features that can enable dose measurements of OARs in PRRT for treating NETs. To meet this aim, we evaluated multiple ML-based prediction algorithms and corresponding dose escalation-associated factors. We investigated the predictive usefulness of 3D radiomic features extracted from each patient's pretreatment and posttreatment dose maps and developed a model that incorporated anatomical radiomic and dosiomic features to predict the absorbed dose in each OAR in patients with NETs treated with  $^{177}\text{Lu}$ -DOTATATE at 24 h.

To the best of our knowledge, this is the first study to develop a dosimetry ML-based model in patients undergoing treatment of NETs with  $^{177}\text{Lu}$ -DOTATATE. To ensure the safety of  $^{177}\text{Lu}$ -DOTATATE therapy, we devised a cutting-edge personalized, OAR-based dosimetry approach for monitoring radiotoxicity throughout long-term treatment (>31 weeks) while also identifying associated patient-based clinical characteristics with the highest prognostic value.

In the proposed methodology for treatment planning described herein, after evaluating nine ML regression algorithms, our model scored a mean absolute dose error of 0.61 for the liver (by gradient boost regressor), 1.58 for the spleen (by extra tree regressor), 1.30 for the left kidney (by gradient boost regressor), and 1.35 for the right kidney (by gradient boost regressor) between pretherapy  $^{68}\text{Ga}$ -DOTATOC PET/CT and posttherapy  $^{177}\text{Lu}$ -DOTATATE SPECT/CT scans. Evaluation of the best regression algorithm for each OAR based on its ability to predict the absorbed dose in each and every pretherapy combination of  $^{68}\text{Ga}$ -DOTATOC PET/CT and any post-therapy  $^{177}\text{Lu}$ -DOTATATE treatment cycle scans, as well as any subsequent  $^{177}\text{Lu}$ -DOTATATE SPECT/CT scans after a  $^{177}\text{Lu}$ -DOTATATE treatment cycle, showed mean differences, between the predicted absorbed dose values and ground truth (MC simulations), less than 1 Gy, ranges from  $-0.55$  to  $0.68$  Gy. Furthermore, using results of initial treatment cycles as input absorbed dose differences in a single time point tended to decrease along with their corresponding SDs. PET studies have shown that pretreatment  $^{68}\text{Ga}$ -DOTATOC PET scans may be useful in determining the optimal activity, and consequently the absorbed dose, for PRRT.<sup>38,39,68</sup> Training our model without considering features extracted from the pretherapy  $^{68}\text{Ga}$ -DOTATOC PET/CT scans was not investigated. Our focus was on developing a comprehensive pretreatment planning dose predictive model that would incorporate the highly promising predictive ability of the pretherapy scans, as demonstrated in previous studies.<sup>42–45</sup>

Although SPECT or PET imaging can offer valuable information about the distribution of radioactivity within the tissue, the absorbed dose map provides more direct information about the actual radiation dose that

the tissue receives. This is particularly important for short-range beta emitters like Lu-177, which primarily deposit their radiation energy locally in the tissue with minimal gamma radiation emission. To ensure the model's accuracy, we used training datasets derived from MC simulations, providing ground truth information. By analyzing the absorbed dose map, regions receiving the desired dose can be identified and the treatment plan can be adjusted, potentially improving efficacy and minimizing side effects. We achieved this by exploiting sophisticated ML-based regression algorithms to personalize the proposed PRRT treatment plan for patients with NETs. We chose not to limit the issue to a simple, straightforward linear regression problem of dose values, like Chicheportiche et al.<sup>37</sup> did, but rather to also correlate doses to OARs with patient-specific and dose distribution-specific characteristics in every possible treatment session for every OAR.

Previous studies presented in the Introduction section relied on linear regression models.<sup>37,44</sup> In contrast, we demonstrated that non-linear-based ML models produce more accurate results of dose prediction for PRRT that do linear-based ML models. Owing to their interpretability and resistance to overfitting with complex, high-dimensional data sets, non-linear-based algorithms (gradient boost or extra tree regressor) proved to be more capable of producing precise predictions with greater capacity for generalization than were linear algorithms.

Both ML and DL based treatment plans have shown remarkable predictive ability in nuclear medicine.<sup>36,69,70</sup> We aimed to develop a model that can predict the absorbed dose from pretreatment imaging sessions but additionally identify patient- and dose-specific features for the purpose of discovering possible correlations between these features. These features can only be identified using ML-based models. As shown in Table 3, wavelet-based features had high predictive value. Although anatomical-based features are less than the dosiomics features, anatomical CT-based features and the patient's body mass index (for the spleen, the left and the right kidney) were highly correlated features. Of note, for every specific target OAR, features of at least two other OARs had an impact on predicting the absorbed dose in the target OAR. These findings not only prove that it is feasible to predict dose relations from pretreatment scans, but also highlight the need for further studies to investigate the correlation between OARs.

#### 4.1 | Limitations

Although our study yielded substantial and encouraging results, it had some limitations. First and foremost, the patient cohort was limited because of COVID-19-related issues that precluded some patients from completing

all four cycles of  $^{177}\text{Lu}$ -DOTATATE therapy. Also, the participating clinics did not follow the exact same scanning protocol after the therapy, as follow-up SPECT/CT scans post therapy are not mandatory. The challenge in gathering integrated follow-up data on patients' scans stems primarily from the fact that no protocol requires  $^{177}\text{Lu}$ -DOTATATE SPECT/CT for any patient after PRRT for NETs. In addition, as a result of the not-mandatory posttreatment scans, we could not acquire all of the posttreatment  $^{177}\text{Lu}$ -DOTATATE SPECT/CT scans for some patients. By using ML-based methods, we adapted to a limited data set. Augmenting our dataset in the future will further verify and standardize our identified features' findings. The results for our prediction model may be impacted by imbalance in its training owing to the number of missed treatment sessions. Furthermore, even though a study by Sandström et al.<sup>7</sup> showed that the absorbed dose in bone marrow is seldom a limiting factor to complete the treatment; several recent studies have emphasized the importance of the bone marrow as an OAR, which may influence the treatment.<sup>2,71,72</sup> We did not investigate the radiodosiomic correlation between pretherapy and posttherapy treatment sessions with bone marrow as an OAR in the present study, although we can study it in the future. In our study, scans were taken from different PET or SPECT/CT scanners with potential variations in image reconstruction protocols and different scanning parameters. Augmenting a data set with data from different hospitals would boost the model's generalization ability and make its results more applicable to other studies. Additionally, the potential of the combination of radiomic and dosiomic features has yet to be described in the literature or demonstrated clinically. Therefore, conclusive interpretation of feature sets composition is lacking. We did not examine different feature extraction parameterization or selection approaches, so an emphasis on specific features may have produced different outcomes. We anticipate that divergent results might emerge if we train our models on radiomic features derived from the raw PET or SPECT activity maps, rather than the generated high-resolution dose maps. Moreover, assumptions were made regarding constant effective half-life, and the use of a single time point for dosimetry prediction. As this study was focused on standardizing an AI methodology for dosimetry prediction, we aimed to introduce an alternative dosimetry procedure for NETs treatment by utilizing a ML-based model. To achieve this, we executed MC simulations on post-injection SPECT/CT scans at an indicative specific time point for every treatment cycle, to standardize the performance of the prediction model. Our model's predictive ability may be further enhanced by time-activity curves to calculate cumulative dose incorporating pharmacokinetics. The  $X_{90}$ , radius of the sphere in which 90% of the beta-emitter's energy is deposited, of Lu-177 in water is 0.6 mm<sup>73</sup> while in our study the dose maps had a voxel size of  $1 \times 1 \times 1$

mm<sup>3</sup>. As we are performing dosimetry in organ level, we anticipate that these differences would not significantly impact the dosimetry prediction, but this is a work that needs to be further investigated in a future study. Finally, patients' laboratory test results (e.g., hematological and biochemical tests) are not integrated into our ML prediction model. Future research should focus on the relationship between radiodosimics and laboratory test results. This may also improve the model's predictive ability and adoption in clinical practice. In this study we evaluated and standardized the proposed prediction model, and we didn't clinically investigate the cumulative absorbed dose over the cycles. The proposed model may be further exploited in clinical dosimetry, predicting the total cumulative dose for all the treatment cycles.

As shown in several published studies,<sup>74,75</sup> radiomic features highlight the complementary value of texture in improving models' accuracies on predicting absorbed dose. Our findings further emphasize the need for developing individualized, data-driven risk profiles in prediction models for PRRT because they strongly depend on patient-specific characteristics, such as the patient's body mass index. Our results demonstrate that the ML-based model's prediction performance can be influenced considerably by the radiodosiomic feature selection technique and regression model used. Simple linear regression models cannot outperform non-linear-based ML models like gradient descent or support vector machines using clinical data sets with limited data. More research is needed before we can make firm conclusions about the effective use of automated models in nuclear molecular radiotherapy and, eventually, development of a precise, patient-specific treatment plan for PRRT in NETs.

## 5 | CONCLUSIONS

Our findings described herein will help future studies to develop optimized MRT approaches for patients with NETs in a prospective manner. For effective tailored dosimetry, an accurate planning agent must be used prior to  $^{177}\text{Lu}$ -DOTATATE therapy. The absorbed dose predicted using the planning agent must correspond with the absorbed dose from the therapeutic isotope ( $^{68}\text{Ga}$ -DOTATOC and  $^{177}\text{Lu}$ -DOTATATE in our study). A dosimetry plan before treatment overall and during  $^{177}\text{Lu}$ -DOTATATE therapy in particular, that is, sufficiently accurate would allow for the selection of optimal activity levels that provide the highest probability of successful tumor suppression for each therapy cycle while also reducing radiation-induced harm to healthy tissues. Thus, by refining the absorbed dose estimation with proper radiomics and dosiomic features and improving the safety and efficacy of  $^{177}\text{Lu}$ -DOTATATE therapy, NET patient outcomes may improve. In future research, investigators should analyze more patient data than we

did in this study to verify this model for use in regular clinical practice.

## ACKNOWLEDGMENTS

The authors appreciate the competent language editing provided by The University of Texas MD Anderson Cancer Center Editing Services, Research Medical Library. This research is co-financed by: a) European Union's Horizon 2020 research and innovation programme under the Marie Skłodowska-Curie grant agreement No 872735. The results published in this study reflect only the author's view and the Research Executive Agency (REA) and the European Commission is not responsible for any use that may be made of the information it contains, b) the [European Regional Development Fund \(ERDF\)](#), Greek General Secretariat for Research and Innovation, Operational Programme "Competitiveness, Entrepreneurship and Innovation" (EPANEK), under the frame of ERA PerMed (project POPEYE T11EPA4-00055), and c) the [Hellenic Foundation for Research and Innovation \(H.F.R.I.\)](#) under the "2nd call for H.F.R.I. research projects to support faculty members & researchers" (project number: 2692). The publication of the article in OA mode was financially supported by HEAL-Link.

## CONFLICT OF INTEREST

The authors have no conflicts to disclose.

## DATA AVAILABILITY STATEMENT

Authors are not able to share data at this time.

## REFERENCES

- Bodei L, Kidd M, Baum RP, Modlin IM. PRRT: defining the paradigm shift to achieve standardization and individualization. *J Nucl Med*. 2014;55(11):1753-1756.
- Del Olmo-Garcia MI, Prado-Wohlwend S, Bello P, Segura A, Merino-Torres JF. Peptide receptor radionuclide therapy with [(177)Lu]Lu-DOTA-TATE in patients with advanced GEP NENS: present and future directions. *Cancers (Basel)*. 2022;14(3):584.
- Puliani G, Chiefari A, Mormando M, Bianchini M, Lauretta R, Appetecchia M. New Insights in PRRT: lessons from 2021. *Front Endocrinol (Lausanne)*. 2022;13:861434.
- Plachouris D, Mountris KA, Papadimitroulas P, et al. Clinical evaluation of a three-dimensional internal dosimetry technique for liver radioembolization with (90)Y microspheres using dose Voxel Kernels. *Cancer Biother Radiopharm*. 2021;36(10):809-819.
- Lu X, Lu C, Yang Y, et al. Current status and trends in peptide receptor radionuclide therapy in the past 20 years (2000-2019): a bibliometric study. *Front Pharmacol*. 2021;12:624534.
- Sgouros G, Dewaraja YK, Escorcia F, et al. Tumor response to radiopharmaceutical therapies: the knowns and the unknowns. *J Nucl Med*. 2021;62(suppl 3):12S-22S.
- Sandstrom M, Garske-Roman U, Granberg D, et al. Individualized dosimetry of kidney and bone marrow in patients undergoing Lu-177-DOTA-Octreotate treatment. *J Nucl Med*. 2013;54(1):33-41.
- Sundlov A, Sjogreen-Gleisner K, Svensson J, et al. Individualised (177)Lu-DOTATATE treatment of neuroendocrine tumours based on kidney dosimetry [published online ahead of print 20170322]. *Eur J Nucl Med Mol Imaging*. 2017;44(9):1480-1489.
- Sundlov A, Gleisner KS, Tennvall J, et al. Phase II trial demonstrates the efficacy and safety of individualized, dosimetry-based (177)Lu-DOTATATE treatment of NET patients [published online ahead of print 20220422]. *Eur J Nucl Med Mol Imaging*. 2022;49(11):3830-3840.
- Svensson J, Berg G, Wangberg B, Larsson M, Forssell-Aronsson E, Bernhardt P. Renal function affects absorbed dose to the kidneys and haematological toxicity during (1)(7)(7)Lu-DOTATATE treatment [published online ahead of print 20150206]. *Eur J Nucl Med Mol Imaging*. 2015;42(6):947-955.
- Yao JC, Hassan M, Phan A, et al. One hundred years after "carcinoid": epidemiology of and prognostic factors for neuroendocrine tumors in 35,825 cases in the United States. *J Clin Oncol*. 2008;26(18):3063-3072.
- Ahmed A, Turner G, King B, et al. Midgut neuroendocrine tumours with liver metastases: results of the UKINETS study [published online ahead of print 2009/05/22]. *Endocr Relat Cancer*. 2009;16(3):885-894.
- Modlin IM, Kidd M, Latich I, Zikusoka MN, Shapiro MD. Current status of gastrointestinal carcinoids [published online ahead of print 2005/05/12]. *Gastroenterology*. 2005;128(6):1717-1751.
- Kwekkeboom DJ, de Herder WW, Kam BL, et al. Treatment with the radiolabeled somatostatin analog [177 Lu-DOTA 0,Tyr3]octreotate: toxicity, efficacy, and survival. *J Clin Oncol*. 2008;26(13):2124-2130.
- Strosberg J, El-Haddad G, Wolin E, et al. Phase 3 trial of (177)Lu-dotatate for midgut neuroendocrine tumors. *N Engl J Med*. 2017;376(2):125-135.
- Strosberg JR, Caplin ME, Kunz PL, et al. Final overall survival in the phase 3 NETTER-1 study of lutetium-177-DOTATATE in patients with midgut neuroendocrine tumors. *J. Clin. Oncol*. 2021;39(15\_suppl):4112.
- Kwekkeboom DJ, Teunissen JJ, Bakker WH, et al. Radiolabeled somatostatin analog [177Lu-DOTA0,Tyr3]octreotate in patients with endocrine gastroenteropancreatic tumors. *J Clin Oncol*. 2005;23(12):2754-2762.
- Jahn U, Ilan E, Sandstrom M, Lubberink M, Garske-Roman U, Sundin A. Peptide receptor radionuclide therapy (PRRT) with Lu-177-DOTATATE; differences in tumor dosimetry, vascularity and lesion metrics in pancreatic and small intestinal neuroendocrine neoplasms. *Cancers*. 2021;13(5):962.
- Lambin P, Rios-Velazquez E, Leijenaar R, et al. Radiomics: extracting more information from medical images using advanced feature analysis. *Eur J Cancer*. 2012;48(4):441-446.
- Patyk M, Silicki J, Mazur R, Krecichwost R, Sokolowska-Dabek D, Zaleska-Dorobisz U. Radiomics—the value of the numbers in present and future radiology. *Pol J Radiol*. 2018;83:e171-e174.
- Papadimitroulas P, Brocki L, Christopher Chung N, et al. Artificial intelligence: deep learning in oncological radiomics and challenges of interpretability and data harmonization. *Phys Med*. 2021;83:108-121.
- Visvikis D, Cheze Le Rest C, Jaouen V, Hatt M. Artificial intelligence, machine (deep) learning and radio(geno)mics: definitions and nuclear medicine imaging applications. *Eur J Nucl Med Mol Imaging*. 2019;46(13):2630-2637.
- Gabrys HS, Buettner F, Sterzing F, Hauswald H, Bangert M. Design and selection of machine learning methods using radiomics and dosiomics for normal tissue complication probability modeling of Xerostomia. *Front Oncol*. 2018;8:35.
- Liang B, Yan H, Tian Y, et al. Dosiomics: extracting 3D spatial features from dose distribution to predict incidence of radiation pneumonitis. *Front Oncol*. 2019;9:269.
- Chopra N, Dou T, Sharp G, Sajo E, Mak RH. A combined radiomics-dosiomics machine learning approach improves prediction of radiation pneumonitis compared to DVH data in lung cancer patients. *Int J Radiat Oncol Biol Phys*. 2020;108:e777.
- Hatt M, Krizsan AK, Rahmim A, et al. Joint EANM/SNMMI guideline on radiomics in nuclear medicine : jointly supported by the

- EANM Physics Committee and the SNMMI Physics, Instrumentation and Data Sciences Council [published online ahead of print 20221103]. *Eur J Nucl Med Mol Imaging*. 2023;50(2):352-375.
27. Qin Y, Zhu LH, Zhao W, Wang JJ, Wang H. Review of radiomics- and dosimetrics-based predicting models for rectal cancer [published online ahead of print 20220809]. *Front Oncol*. 2022;12:913683.
  28. Wang B, Liu J, Zhang X, et al. Prognostic value of (18)F-FDG PET/CT-based radiomics combining dosimetrics and dose volume histogram for head and neck cancer [published online ahead of print 20230213]. *EJNMMI Res*. 2023;13(1):14.
  29. Baum RP, Kulkarni HR, Singh A, et al. Results and adverse events of personalized peptide receptor radionuclide therapy with (90)Yttrium and (177)Lutetium in 1048 patients with neuroendocrine neoplasms. *Oncotarget*. 2018;9(24):16932-16950.
  30. Kesavan M, Turner JH. Myelotoxicity of peptide receptor radionuclide therapy of neuroendocrine tumors: a decade of experience. *Cancer Biother Radiopharm*. 2016;31(6):189-198.
  31. Sabet A, Ezziddin K, Pape UF, et al. Long-term hematotoxicity after peptide receptor radionuclide therapy with Lu-177-Octreotate. *J Nucl Med*. 2013;54(11):1857-1861.
  32. Arabi H, Zaidi H. Applications of artificial intelligence and deep learning in molecular imaging and radiotherapy. *Eur J Hybrid Imag*. 2020;4(1):17.
  33. Mazurowski MA. Artificial intelligence may cause a significant disruption to the radiology workforce. *J Am Coll Radiol*. 2019;16(8):1077-1082.
  34. Yi PH, Hui FK, Ting DSW. Artificial intelligence and radiology: collaboration is key. *J Am Coll Radiol*. 2018;15(5):781-783.
  35. Decuyper M, Maebe J, Van Holen R, Vandenberghe S. Artificial intelligence with deep learning in nuclear medicine and radiology. *Ejnmms Phys*. 2021;8(1):81.
  36. Plachouris D, Tzolas I, Gatos I, et al. A deep-learning-based prediction model for the biodistribution of (90)Y microspheres in liver radioembolization. *Med Phys*. 2021;48(11):7427-7438.
  37. Chicheportiche A, Grozinsky-Glasberg S, Gross DJ, et al. Predictive power of the post-treatment scans after the initial or first two courses of [Lu-177]-DOTA-TATE. *Ejnmms Phys*. 2018;5(1):36.
  38. Akhavanallah A, Peterson AB, Fitzpatrick K, et al. The predictive value of pretherapy [(68)Ga]Ga-DOTA-TATE PET and biomarkers in [(177)Lu]Lu-PRRT tumor dosimetry [published online ahead of print 20230512]. *Eur J Nucl Med Mol Imaging*. 2023;50(10):2984-2996.
  39. Bruvold R, Blakkisrud J, Mikalsen LT, Connelly J, Stokke C. Correlations between [(68)Ga]Ga-DOTA-TOC Uptake and Absorbed Dose from [(177)Lu]Lu-DOTA-TATE [published online ahead of print 20230210]. *Cancers (Basel)*. 2023;15(4):1134.
  40. Kratochwil C, Stefanova M, Mavriopoulou E, et al. SUV of [68Ga]DOTATOC-PET/CT predicts response probability of prrt in neuroendocrine tumors. *Mol Imaging Biol*. 2015;17(3):313-318.
  41. Sharma R, Wang WM, Yusuf S, et al. Ga-DOTATATE PET/CT parameters predict response to peptide receptor radionuclide therapy in neuroendocrine tumours. *Radiother Oncol*. 2019;141:108-115.
  42. Thuillier P, Maajem M, Schick U, et al. Clinical assessment of 177Lu-DOTATATE quantification by comparison of SUV-based parameters measured on both Post-PRRT SPECT/CT and 68Ga-DOTATOC PET/CT in patients with neuroendocrine tumors: a feasibility study. *Clin Nucl Med*. 2021;46(2):111-118.
  43. Ezziddin S, Lohmar J, Yong-Hing CJ, et al. Does the pretherapeutic tumor SUV in 68Ga DOTATOC PET predict the absorbed dose of 177Lu octreotate? *Clin Nucl Med*. 2012;37(6):e141-147.
  44. Kim YI, Oh J, Yoo C, Ryoo BY, Ryu JS. Prediction of absorbed dose by tumors and critical organs after Lu-177-DOTATATE therapy using pretherapeutic Ga-68-DOTATOC PET/CT. *J Nucl Med*. 2021;62(supplement 1):76.
  45. Wong KK, Frey KA, Niedbala J, et al. Differences in tumor-to-normal organ SUV ratios measured with 68 Ga-DOTATATE PET compared with 177 Lu-DOTATATE SPECT in patients with neuroendocrine tumors [published online ahead of print 20220610]. *Nucl Med Commun*. 2022;43(8):892-900.
  46. Vergnaud L, Giraudet AL, Moreau A, et al. Patient-specific dosimetry adapted to variable number of SPECT/CT time-points per cycle for [Formula: see text]Lu-DOTATATE therapy [published online ahead of print 2022/05/17]. *Ejnmms Phys*. 2022;9(1):37.
  47. Dewaraja YK, Frey EC, Sgouros G, et al. MIRDO pamphlet No. 23: quantitative SPECT for patient-specific 3-dimensional dosimetry in internal radionuclide therapy [published online ahead of print 20120628]. *J Nucl Med*. 2012;53(8):1310-1325.
  48. Pedregosa F, Varoquaux G, Gramfort A, et al. Scikit-learn: machine Learning in Python. *J Mach Learn Res*. 2011;12:2825-2830.
  49. Chen T, Guestrin C. XGBoost: a Scalable Tree Boosting System. 22nd SIGKDD Conference on Knowledge Discovery and Data Mining; 2016:785-794.
  50. Van Rossum G, Drake Jr FL. *Python Reference Manual*. Centrum voor Wiskunde en Informatica; 1995.
  51. van Griethuysen JJM, Fedorov A, Parmar C, et al. Computational radiomics system to decode the radiographic phenotype. *Cancer Res*. 2017;77(21):E104-E107.
  52. Hatt M, Vallieres M, Visvikis D, Zwanenburg A. IBSI: an international community radiomics standardization initiative. *J Nucl Med*. 2018;59(supplement 1):287.
  53. Afshar P, Mohammadi A, Plataniotis KN, Oikonomou A, Benali H. From handcrafted to deep-learning-based cancer radiomics challenges and opportunities. *IEEE Signal Proc Mag*. 2019;36(4):132-160.
  54. Lipton ZC. The Mythos of model interpretability. *Commun ACM*. 2018;61(10):36-43.
  55. *P4P: Pearson's correlation coefficient*. In: Kirch W, ed. *Encyclopedia of Public Health*; 2008.
  56. Shannon C. A mathematical theory of communication. *ACM SIGMOBILE Mobile Comput Commun Rev*. 2001;5(1):3-55.
  57. Kullback S, Leibler RA. On information and sufficiency. *Ann Math Statist*. 1951;22(1):79-86.
  58. LOOCV. Leave-One-Out cross-validation. In: C/S, ed. *Encyclopedia of Machine Learning*. Springer; 2011.
  59. Willmott CJ, Matsuura K. Advantages of the mean absolute error (MAE) over the root mean square error (RMSE) in assessing average model performance. *Climate Res*. 2005;30(1):79-82.
  60. Sarrut D, Bardies M, Bousson N, et al. A review of the use and potential of the GATE Monte Carlo simulation code for radiation therapy and dosimetry applications. *Med Phys*. 2014;41(6):064301.
  61. Sarrut D, Arbor N, Baudier T, et al. The OpenGATE ecosystem for Monte Carlo simulation in medical physics [published online ahead of print 20220908]. *Phys Med Biol*. 2022;67(18):184001.
  62. Computing YA. *High-Performance Computing (HPC) Center*. Accessed July 21, 2023. <https://www.yac.hr/>
  63. Webb GI. *Encyclopedia of Machine Learning*. Springer; 2010.
  64. Bodei L, Cremonesi M, Ferrari M, et al. Long-term evaluation of renal toxicity after peptide receptor radionuclide therapy with Y-90-DOTATOC and Lu-177-DOTATATE: the role of associated risk factors. *Eur J Nucl Med Mol I*. 2008;35(10):1847-1856.
  65. Frilling A, Modlin IM, Kidd M, et al. Recommendations for management of patients with neuroendocrine liver metastases. *Lancet Oncol*. 2014;15(1):E8-E21.
  66. Kwekkeboom DJ, Mueller-Brand J, Paganelli G, et al. Overview of results of peptide receptor radionuclide therapy with 3 radiolabeled somatostatin analogs. *J Nucl Med*. 2005;46:62s-66s.
  67. Sabet A, Dautzenberg K, Haslerud T, et al. Specific efficacy of peptide receptor radionuclide therapy with Lu-177-octreotate in advanced neuroendocrine tumours of the small intestine. *Eur J Nucl Med Mol I*. 2015;42(8):1238-1246.

68. Peterson AB, Wang C, Wong KK, et al.  $^{177}\text{Lu}$ -DOTATATE theranostics: predicting renal dosimetry from pretherapy  $^{68}\text{Ga}$ -DOTATATE PET and clinical biomarkers [published online ahead of print 20230208]. *Clin Nucl Med*. 2023;48(5):393-399.
69. Lee MS, Hwang D, Kim JH, Lee JS. Deep-dose: a voxel dose estimation method using deep convolutional neural network for personalized internal dosimetry. *Sci Rep-Uk*. 2019;9:10308.
70. Eleftheriadis V, Savvidis G, Paneta V, Chatzipapas K, Kagadis GC, Papadimitroulas P. A framework for prediction of personalized pediatric nuclear medical dosimetry based on Machine Learning and Monte Carlo techniques [published online ahead of print 20230315]. *Phys Med Biol*. 2023; 68(8):084004. doi:10.1088/1361-6560/acc4a5
71. Sansovini M, Severi S, Ambrosetti A, et al. Treatment with the radiolabelled somatostatin analog Lu-177-DOTATATE for advanced pancreatic neuroendocrine tumors. *Neuroendocrinology*. 2013;97(4):347-354.
72. Wehrmann C, Senftleben S, Zachert C, Muller D, Baum RP. Results of individual patient dosimetry in peptide receptor radionuclide therapy with Lu-177 DOTA-TATE and Lu-177 DOTA-NOC. *Cancer Biother Radio*. 2007;22(3):406-416.
73. Stokke C, Kvasheim M, Blakkisrud J. Radionuclides for targeted therapy: physical properties [published online ahead of print 20220825]. *Molecules*. 2022;27(17):5429.
74. Fave X, Zhang LF, Yang JZ, et al. Impact of image preprocessing on the volume dependence and prognostic potential of radiomics features in non-small cell lung cancer. *Transl Cancer Res*. 2016;5(4):349-363.
75. Yip SSF, Aerts HJWL. Applications and limitations of radiomics. *Phys Med Biol*. 2016;61(13):R150-R166.

**How to cite this article:** Plachouris D, Eleftheriadis V, Nanos T, et al. A radiomic- and dosiomic-based machine learning regression model for pretreatment planning in  $^{177}\text{Lu}$ -DOTATATE therapy. *Med Phys*. 2023;1-14. <https://doi.org/10.1002/mp.16746>